Inorg. Chem. **2009**, *48*, 2844−2854

Theoretical Studies on Metal−Metal Interaction, Excited States, and Spectroscopic Properties of Binuclear Au−Au, Au−Rh, and Rh−Rh Complexes with Diphosphine Ligands: Buildup of Complexity from Monomers to Dimers

Qing-Jiang Pan,[†] Xin Zhou,[§] Yuan-Ru Guo,[‡] Hong-Gang Fu,[†,*] and Hong-Xing Zhang[§,*]

Laboratory of Physical Chemistry and Key Laboratory of Functional Inorganic Material Chemistry of Education Ministry, School of Chemistry and Materials Science, Heilongjiang University, Harbin 150080, China, College of Material Science and Engineering, Northeast Forestry University, Harbin 150040, China, and State Key Laboratory of Theoretical and Computational Chemistry, Institute of Theoretical Chemistry, Jilin University, Changchun 130023, China

Received September 2, 2008

To understand their photocatalytic activity and application in luminescent materials, a series of gold and rhodium phosphine complexes (mononuclear $[Au^{I}(PH_3)_2]^+$ (**1**) and $[Rh^{I}(CNH)_2(PH_3)_2]^+$ (**2**); homobinuclear $[Au^{I}_2(PH_2CH_2PH_2)_2]^{2+}$ (**3**)and$[Rh^{I}_2(CNH)_4(PH_2CH_2PH_2)_2]^{2+}$(**4**);heterobinuclear$[Au^{I}Rh^{I}(CNH)_2(PH_2CH_2PH_2)_2]^{2+}$(**5**),$[Au^{I}Rh^{I}(CNH)_2(PH_2NHPH_2)_2Cl_2]$ (**6**), and $[Au^{I}Rh^{I}(CNH)_2(PH_2NHPH_2)_2]^{2+}$ (**7**); and oxidized derivatives $[Au^{II}Rh^{II}(CNH)_2(PH_2CH_2PH_2)_2]^{4+}$ (**8**), $[Au^{II}Rh^{II}(CNH)_2(PH_2NHPH_2)_2Cl_3]^+$ (**9**), and $[Au^{II}Rh^{II}(CNH)_2(PH_2NHPH_2)_2]^{4+}$ (**10**)) were investigated using ab initio methods and density functional theory. With the use of the MP2 method, the M−M′ distances in **3**−**7** were estimated to be in the range of 2.76−3.02 Å, implying the existence of weak metal−metal interaction. This is further evident in the stretching frequencies and bond orders of M−M′. The two-electron oxidation from **5**−**7** to their respective partners **8**−**10** was shown to mainly occur in the gold−rhodium centers. Experimental absorption spectra were well reproduced by our time-dependent density functional theory calculations. The metal−metal interaction results in a large shift of $d_{z^2} \rightarrow p_z$ transition absorptions in binuclear complexes relative to mononuclear analogues and concomitantly produces a low-lying excited state that is responsible for increasing visible-light photocatalytic activities. Upon excitation, the metal-centered transition and the metal-to-metal charge transfer strengthen the metal−metal interaction in triplet excited states for **3**−**6**, while the promotion of electrons into the $\sigma^*(d_{z^2})$ orbital weakens the interaction in **9**.

1. Introduction

The absorption of light during the metal-centered $d \rightarrow p$ transition leads to phosphorescence in mononuclear d^{10} gold(I), silver(I), and copper(I) complexes.[1] Usually, these complexes luminesce in solid states but not dilute solutions. Experimental[2−4] and theoretical[3−6] investigations have shown

* To whom correspondence should be addressed. E-mail: fuhg@vip.sina.com (H.-G.F.), zhanghx@mail.jlu.edu.cn (H.-X.Z.).
† Heilongjiang University.
‡ Northeast Forestry University.
§ Jilin University.

(1) (a) Che, C.-M.; Chao, H.-Y.; Miskowski, V. M.; Li, Y.; Cheung, K.-K. *J. Am. Chem. Soc.* **2001**, *123*, 4985–4991. (b) Lu, W.; Xiang, H.-F.; Zhu, N.; Che, C.-M. *Organometallics* **2002**, *21*, 2343–2346. (c) Narayanaswamy, R.; Young, M. A.; Parkhurst, E.; Ouellette, M.; Kerr, M. E.; Ho, K. M.; Elder, R. C.; Bruce, A. E.; Bruce, M. R. M. *Inorg. Chem.* **1993**, *32*, 2506–2517. (d) Jones, W. B.; Yuan, J.; Narayanaswamy, R.; Young, M. A.; Elder, R. C.; Bruce, A. E.; Bruce, M. R. M. *Inorg. Chem.* **1995**, *34*, 1996–2001.

(2) (a) Mansour, M. A.; Connick, W. B.; Lachicotte, R. J.; Gysling, H. J.; Eisenberg, R. *J. Am. Chem. Soc.* **1998**, *120*, 1329–1330. (b) Lee, Y. A.; McGarrah, J. E.; Lachicotte, R. J.; Eisenberg, R. *J. Am. Chem. Soc.* **2002**, *124*, 10662–10663. (c) Schmidbaur, H.; Cronje, S.; Djordjevic, B.; Schuster, O. *Chem. Phys.* **2005**, *311*, 151–161. (d) Fackler, J. P., Jr. *Inorg. Chem.* **2002**, *41*, 6959–6972.

(3) Rawashdeh-Omary, M. A.; Omary, M. A.; Patterson, H. H.; Fackler, J. P., Jr. *J. Am. Chem. Soc.* **2001**, *123*, 11237–11247.

(4) Fernández, E. J.; López-de-Luzuraga, J. M.; Monge, M.; Rodríguez, M. A.; Crespo, O.; Gimeno, M. C.; Laguna, A.; Jones, P. G. *Inorg. Chem.* **1998**, *37*, 6002–6006.

(5) Schwerdtfeger, P.; Bruce, A. E.; Bruce, M. R. M. *J. Am. Chem. Soc.* **1998**, *120*, 6587–6597.

(6) (a) Pan, Q.-J.; Zhou, X.; Fu, H.-G.; Zhang, H.-X. *Organometallics* **2008**, *27*, 2474–2482. (b) Pan, Q.-J.; Zhang, H.-X. *Inorg. Chem.* **2004**, *43*, 593–601.

10.1021/ic801687w CCC: $40.75
Published on Web 03/12/2009

that metal−metal interaction plays an important role in determining luminescence. The weak $d^{10}-d^{10}$ interactions have been termed *metallophilicity*.[7−9] The energy for Au(I)−Au(I) aurophilicity has been estimated as 7−15 kcal/mol, which is comparable to that of hydrogen bonds.[10] Pyykkö and Mendizabal attributed the aurophilicity to correlation effects, strengthened by relativistic effects.[11] To reveal the relationship between metallophilic interaction and luminescence, complexes containing gold(I) with bridging ligands are ideal candidates for representing bimetallic complexes.[2,4,6−9] Special attention has been focused on binuclear Au(I) diphosphine complexes, which exhibit intense metal-localized $\sigma^*(d) \rightarrow \sigma(p)$ electronic spectroscopy and a predominant Au−Au contraction in the low-lying excited state.[6−12]

Metal−metal interaction and luminescence are also present in d^8 complexes such as Rh(I),[13−18] Ir(I),[16,18a,19] Pt(II),[20−23] Pd(II),[24] and Ni(II).[22a,25] It is well-known that rhodium complexes are widely used as photocatalysts. Housecroft[26] and Nocera and Esswein[27] have reviewed existing and potential applications using rhodium complexes. Mononuclear catalysts require higher-energy ultraviolet-light irradiation. If a Rh−Rh interaction is introduced into a molecular system, the excitation energy lowers, and the visible-light photocatalyst becomes available. For example, the paddlewheel-structured $[Rh^{I}_2(diprop)_4]^{2+}$ complex (diprop = 1,3-diisocyanopropane) was reported to have a reactive excited state.[16a] Irradiation at 546 nm in aqueous solutions of hydrohalic acids (HX) results in the production of H_2 and the formation of a d^7-d^7 $[Rh^{II}_2(diprop)_4X_2]^{2+}$ species. This complex has also been considered as a candidate for solar energy conversion devices owing to its relatively long phosphorescence lifetime.[16] Therefore, metal−metal interactions not only lower the excitation energy but produce a steady low-lying excited state to promote the photocatalytic activity of binuclear rhodium complexes in the visible region.

Since gold(I) complexes are light-sensitive and rhodium(I) ones are highly photocatalytic, their combination may present an attractive photocatalyst. The combination involves a low-lying excited state due to the Au−Rh interaction, and its photochemical reaction can be initiated by visible light. Recently, Nocera et al. have characterized two Au(I)−Rh(I) complexes, C-bridged diphosphine $[Au^{I}Rh^{I}(CN^{t}Bu)_2(PPh_2CH_2Ph_2)_2]\cdot Cl_2$[28] and N-bridged diphosphine $[Au^{I}Rh^{I}(CN^{t}Bu)_2(P(OCH_2CF_3)_2NMeP(OCH_2CF_3)_2)_2Cl_2]$,[29] with Au−Rh distances of 2.921 and 2.818 Å, respectively. They display intense $\sigma^*(d) \rightarrow \sigma(p)$ transition spectroscopy[29,30] and exhibit potential photocatalysis for hydrogen production. With the exception of Au(I)−Rh(I) complexes,[28−31] many heteronuclear complexes with closed-shell electronic configurations have been synthesized, such as Au/Rh/Pt−M′ (M′ belongs to $d^6/d^8/d^{10}/s^2$ metal).[32−47]

Currently, computational methods are sufficiently advanced to allow for the calculation of excited states for large molecules.[48,49] Our previous studies were limited to homo-

(7) Che, C.-M.; Lai, S.-W. *Coord. Chem. Rev.* **2005**, *249*, 1296–1309.

(8) (a) Leung, K. H.; Phillips, D. L.; Tse, M.-C.; Che, C.-M.; Miskowski, V. M. *J. Am. Chem. Soc.* **1999**, *121*, 4799–4803. (b) Fu, W.-F.; Chan, K.-C.; Miskowski, V. M.; Che, C.-M. *Angew. Chem., Int. Ed.* **1999**, *38*, 2783–2785. (c) King, C.; Wang, J. C.; Khan, M. N. I.; Fackler, J. P., Jr. *Inorg. Chem.* **1989**, *28*, 2145–2149.

(9) (a) Che, C.-M.; Tse, M.-C.; Chan, M. C. W.; Cheung, K.-K.; Phillips, D. L.; Leung, K.-H. *J. Am. Chem. Soc.* **2000**, *122*, 2464–2468. (b) Che, C.-M.; Mao, Z.; Miskowski, V. M.; Tse, M.-C.; Chan, C.-K.; Cheung, K.-K.; Phillips, D. L.; Leung, K.-H. *Angew. Chem., Int. Ed.* **2000**, *39*, 4084–4088.

(10) (a) Schmidbaur, H. *Chem. Soc. Rev.* **1995**, *24*, 391–400. (b) Schmidbaur, H. *Gold Bull.* **1990**, *23*, 11–21.

(11) (a) Pyykkö, P. *Angew. Chem., Int. Ed.* **2004**, *43*, 4412–4456. (b) Pyykkö, P. *Chem. Rev.* **1997**, *97*, 597–636. (c) Pyykkö, P.; Mendizabal, F. *Inorg. Chem.* **1998**, *37*, 3018–3025. (d) Pyykkö, P. *Science* **2000**, *290*, 64–65.

(12) (a) Zhang, H.-X.; Che, C.-M. *Chem.—Eur. J.* **2001**, *7*, 4887–4893. (b) Pan, Q.-J.; Zhang, H.-X.; Fu, H.-G.; Yu, H.-T. *Eur. J. Inorg. Chem.* **2006**, 1050–1059.

(13) (a) Fordyce, W. A.; Crosby, G. A. *J. Am. Chem. Soc.* **1982**, *104*, 985–988. (b) Balch, A. L. *J. Am. Chem. Soc.* **1976**, *98*, 8049–8054.

(14) (a) Cowie, M.; Dwight, S. K. *Inorg. Chem.* **1980**, *19*, 2500–2507. (b) Mague, J. T. *Inorg. Chem.* **1969**, *8*, 1975–1981. (c) Stace, J. J.; Lambert, K. D.; Krause, J. A.; Connick, W. B. *Inorg. Chem.* **2006**, *45*, 9123–9131. (d) Daws, C. A.; Hill, M. G.; Bullock, J. P.; Mann, K. R. *Inorg. Chem.* **1992**, *31*, 2948–2955. (e) Boyd, D. C.; Matsch, P. A.; Mixa, M. M.; Man, K. R. *Inorg. Chem.* **1986**, *25*, 3331–3333. (f) Mann, K. R.; Thichk, J. A.; Bell, R. A.; Coyle, C. L.; Gray, H. B. *Inorg. Chem.* **1980**, *19*, 2462–2468. (g) Gerlits, O.; Kovalevsky, A. Y.; Coppens, P. *Dalton Trans.* **2004**, *3955*, 3962.

(15) (a) Dallinger, R. F.; Miskowski, V. M.; Gray, H. B.; Woodruff, W. H. *J. Am. Chem. Soc.* **1981**, *103*, 1595–1596. (b) Rice, S. R.; Gray, H. B. *J. Am. Chem. Soc.* **1981**, *103*, 1593–1595. (c) Coppens, P.; Gerlits, O.; Vorontsov, I. I.; Kovalesky, A. Y.; Chen, Y.-S.; Graber, T.; Gembicky, M.; Novozhilova, I. V. *Chem. Commun.* **2004**, *2144*, 2145. (d) Rice, S. F.; Miskowski, V. M.; Gray, H. B. *Inorg. Chem.* **1988**, *27*, 4704–4708.

(16) (a) Harvey, P. D. *Coord. Chem. Rev.* **2001**, *210−221*, 17–52. (b) Man, K. R.; Lewis, N. S.; Miskowski, V. M.; Erwin, D. K.; Hammond, G. S.; Gray, H. B. *J. Am. Chem. Soc.* **1977**, *99*, 5525–5526.

(17) (a) Mann, K. R.; Lewis, N. S.; Willianms, R. M.; Gray, H. B.; Gordon, J. G., II. *Inorg. Chem.* **1978**, *17*, 828–834. (b) Tran, N. T.; Stork, J. R.; Pham, D.; Olmstead, M. M.; Fettinger, J. C.; Balch, A. L. *Chem. Commun.* **2006**, *1130*, 1132.

(18) (a) Geoffroy, G. L.; Wrighton, M. S.; Hammond, G. S.; Gray, H. B. *J. Am. Chem. Soc.* **1974**, *96*, 3105–3108. (b) Jiménez, M. V.; Pérez-Torrente, J. J.; Bartolomé, M. I.; Gierz, V.; Lahoz, F. J.; Oro, L. A. *Organometallics* **2008**, *27*, 224–234.

(19) (a) Mague, J. T.; Devries, S. H. *Inorg. Chem.* **1980**, *19*, 3743–3755. (b) Veige, A. S.; Gray, T. G.; Nocera, D. G. *Inorg. Chem.* **2005**, *44*, 17–26.

(20) (a) Roundhill, D. M.; Gray, H. B.; Che, C.-M. *Acc. Chem. Res.* **1989**, *22*, 55–61. (b) Zipp, A. P. *Coord. Chem. Rev.* **1988**, *84*, 47–83.

(21) (a) King, C.; Auerbach, R. A.; Fronczek, F. R.; Roundhill, D. M. *J. Am. Chem. Soc.* **1986**, *108*, 5626–5627. (b) Roundhill, D. M.; Shen, Z.-P.; King, C.; Atherton, S. J. *J. Phys. Chem.* **1988**, *92*, 4088–4094.

(22) (a) Xia, B.-H.; Che, C.-M.; Phillips, D. L.; Leung, K.-H.; Cheung, K.-K. *Inorg. Chem.* **2002**, *41*, 3866–3875. (b) Che, C.-M.; Yam, V. W.-W.; Wong, W.-T.; Lai, T.-F. *Inorg. Chem.* **1989**, *28*, 2908–2910.

(23) (a) Yam, V. W.-W. *Acc. Chem. Res.* **2002**, *35*, 555–563. (b) Wong, K. M.-C.; Hui, C.-K.; Yu, K.-L.; Yam, V. W.-W. *Coord. Chem. Rev.* **2002**, *229*, 123–132.

(24) (a) Xia, B.-H.; Che, C.-M.; Zhou, Z.-Y. *Chem.—Eur. J.* **2003**, *9*, 3055–3064. (b) Yip, H.-K.; Lai, T.-F.; Che, C.-M. *J. Chem. Soc., Dalton Trans.* **1991**, *1639*, 1641.

(25) Kobayashi, A.; Kojima, T.; Ikeda, R.; Kitagawa, H. *Inorg. Chem.* **2006**, *45*, 322–327.

(26) (a) Housecrosft, C. E. *Coord. Chem. Rev.* **1992**, *115*, 191–230. (b) Housecrosft, C. E. *Coord. Chem. Rev.* **1995**, *146*, 1–281. (c) Housecrosft, C. E. *Coord. Chem. Rev.* **1996**, *152*, 107–139.

(27) Esswein, A. J.; Nocera, D. G. *Chem. Rev.* **2007**, *107*, 4022–4047.

(28) Dempsey, J. L.; Esswein, A. J.; Manke, D. R.; Rosenthal, J.; Soper, J. D.; Nocera, D. G. *Inorg. Chem.* **2005**, *44*, 6879–6892.

(29) Esswein, A. J.; Dempsey, J. L.; Nocera, D. G. *Inorg. Chem.* **2007**, *46*, 2362–2364.

(30) (a) Striplin, D. R.; Crosby, G. A. *J. Phys. Chem.* **1995**, *99*, 11041–11045. (b) Striplin, D. R.; Crosby, G. A. *J. Phys. Chem.* **1995**, *99*, 7977–7984. (c) Yip, H.-K.; Lin, H.-M.; Wang, Y.; Che, C.-M. *Inorg. Chem.* **1993**, *32*, 3402–3407.

(31) (a) McNair, R. J.; Nilsson, P. V.; Pignolet, L. H. *Inorg. Chem.* **1985**, *24*, 1935–1939. (b) Aullón, G.; Alvarez, S. *Inorg. Chem.* **1996**, *35*, 3137–3144.

bimetallic complexes,[6,12,50] rationalizing their metal−metal interaction and luminescent properties. Recently, our aim has been directed toward heterobimetallic complexes.[51] The heterobimetallic Au−Rh complexes indicated earlier are an important and interesting subject toward understanding existing and potential photocatalytic activity and applications in luminescent materials. In this paper, metal−metal interactions in homo- and heterobimetallic complexes were addressed in ground and excited states. Oxidation from Au(I)−Rh(I) species to Au(II)−Rh(II) species was explored theoretically. The influence of isoelectronic CH_2/NH bridgeheads on diphosphine Au−Rh complexes was discussed, and the metal-localized triplet excited states were optimized for mono- and binuclear complexes.

2. Computational Details and Theory

In our calculations, we use the hydrogen atom to represent phenyl, methyl, and *t*butyl groups bonding to the real ligands ($PR_2CH_2PR_2$, $PR_2NR'PR_2$, CNR). A similar simplification has been successfully applied in previous works.[5,6,12,49−52] We theoretically investigated 10 gold and rhodium model complexes, herein referred to by numbers: mononuclear $[Au^I(PH_3)_2]^+$ (**1**) and $[Rh^I(CNH)_2(PH_3)_2]^+$ (**2**); homobinuclear C-bridged $[Au^I_2(PH_2CH_2PH_2)_2]^{2+}$ (**3**) and C-bridged $[Rh^I_2(CNH)_4(PH_2CH_2PH_2)_2]^{2+}$ (**4**); heterobinuclear C-bridged $[Au^IRh^I(CNH)_2(PH_2CH_2PH_2)_2]^{2+}$ (**5**), N-bridged $[Au^IRh^I(CNH)_2(PH_2NHPH_2)_2Cl_2]$ (**6**), and N-bridged $[Au^IRh^I(CNH)_2(PH_2NHPH_2)_2]^{2+}$ (**7**); and heterobinuclear oxidized derivatives $[Au^{II}Rh^{II}(CNH)_2(PH_2CH_2PH_2)_2]^{4+}$ (**8**), $[Au^{II}Rh^{II}(CNH)_2(PH_2NHPH_2)_2Cl_3]^+$ (**9**), and $[Au^{II}Rh^{II}(CNH)_2(PH_2NHPH_2)_2]^{4+}$ (**10**).

We took **5** as the reference sample to compare the performance of various methods, basis sets, and solvent-effect models. First, the MP2, XαVWN, SVWN, PBEPBE, BP86, B3LYP, BH&H, and BH&HLYP methods with three types of basis sets (S-Table 1 of Supporting Information) were employed to optimize the molecular structure. The comparison with experimental values for $[Au^IRh^I(CN^tBu)_2(PPh_2CH_2Ph_2)_2]\cdot Cl_2$[28] shows that the MP2 method combined with BS-III can yield better results (S-Table 2, Supporting Information). Therefore, this approach was used to optimize the ground-state structures of **1**−**10**. Second, the time-dependent density functional theory (TD-DFT)[48−52] and solvent effects were taken into account to obtain reasonable predictions of the absorption spectra. In general, electronic spectroscopy depends strongly on the choice of density functional and solvent-effect model. To look for the optimal method and solvent-effect model, the B3LYP and PBE functionals associated with the C-PCM and PCM models were used to calculate the electronic spectra of **5**. The calculated absorptions and simulated spectra are presented in S-Table 3 and S-Figure 1 (Supporting Information), respectively. Although calculations at all four levels can reflect the general spectral characteristics of the complex, a better agreement with the experimental spectrum was found at the B3LYP/C-PCM level.

Optimizations on **1**−**6** and **9** in triplet excited states were performed at the unrestricted MP2 (UMP2)[53] level. Herein, we adopted C_i symmetry for **1** and **3**; C_{2h} for **2** and **4**; C_2 for **5**, **7**, **8**, and **10**; and C_1 for **6** and **9**. Relativistic effects were considered using Hay and Wadt[54] effective core potentials (ECPs) for Au, Rh, Cl, and P atoms. The LANL2DZ basis sets associated with the ECPs were employed. The 6-31G* basis sets were used for the C, N, and H atoms (S-Table 1, Supporting Information). In order to better describe the molecular properties, an additional function was implemented for Au ($\alpha_f = 0.20$), Rh ($\alpha_f = 0.14$), Cl ($\alpha_d = 0.514$),

(32) (a) Catalano, V. J.; Horner, S. J. *Inorg. Chem.* **2003**, *42*, 8430–8438. (b) Fernández, E. J.; López-de-Luzuriaga, J. M.; Monge, M.; Rodríguez, M. A.; Crespo, L.; Gimeno, M. C.; Laguna, A.; Jones, P. G. *Chem.—Eur. J.* **2000**, *6*, 636–644. (c) Rawashdeh-Omary, M. A.; Omary, M. A.; Fackler, J. P., Jr. *Inorg. Chim. Acta* **2002**, *334*, 376–384.

(33) (a) Wang, S.; Fackler, J. P., Jr. *Organometallics* **1988**, *7*, 2415–2417. (b) Wang, S.; Fackler, J. P., Jr. *Organometallics* **1989**, *8*, 1578–1579. (c) Mardají, M.; Laguna, A. *Eur. J. Inorg. Chem.* **2003**, 3069–3079.

(34) (a) Raptis, R. G.; Porter, L. C.; Emrich, R. J.; Murray, H. H.; Fackler, J. P., Jr. *Inorg. Chem.* **1990**, *29*, 4408–4412. (b) Mazany, A. M.; Fackler, J. P., Jr. *J. Am. Chem. Soc.* **1984**, *106*, 801–802. (c) Méndez, L. A.; Jiménez, J.; Cerrada, E.; Mohr, F.; Laguna, M. *J. Am. Chem. Soc.* **2005**, *127*, 852–853.

(35) (a) Xia, B.-H.; Zhang, H.-X.; Che, C.-M.; Leung, K.-H.; Phillips, D. L.; Zhu, N.; Zhou, Z.-Y. *J. Am. Chem. Soc.* **2003**, *125*, 10362–10374. (b) Yip, H.-K.; Lin, H.-M.; Cheung, K.-K.; Che, C.-M.; Wang, Y. *Inorg. Chem.* **1994**, *33*, 1644–1651. (c) Yin, G.-Q.; Wei, Q.-H.; Zhang, L.-Y.; Chen, Z.-N. *Organometallics* **2006**, *255*, 580–587. (d) Hayoun, R.; Zhong, D. K.; Rheingold, A. L.; Doerrer, L. H. *Inorg. Chem.* **2006**, *45*, 6120–6122.

(36) (a) Fernández, E. J.; Laguna, A.; López-de-Luzuriaga, J. M. *Dalton Trans.* **2007**, *1969*, 1981. (b) Balch, A. L.; Catalano, V. J.; Olmstead, M. M. *Inorg. Chem.* **1990**, *29*, 585–586. (c) Balch, A. L.; Nagle, J. K.; Oram, D. E.; Reedy, P. E., Jr. *J. Am. Chem. Soc.* **1988**, *110*, 454–462. (d) Balch, A. L.; Catalano, V. J.; Olmstead, M. M. *J. Am. Chem. Soc.* **1990**, *112*, 2010–2011.

(37) (a) Balch, A. L.; Noll, B. C.; Olmstead, M. M.; Toronto, D. V. *Inorg. Chem.* **1992**, *31*, 5226–5230. (b) Balch, A. L.; Noll, B. C.; Olmstead, M. M.; Toronto, D. V. *Inorg. Chem.* **1993**, *32*, 3613–3619.

(38) (a) Wang, S.; Garzón, G.; King, C.; Wang, J.-C.; Fackler, J. P., Jr. *Inorg. Chem.* **1989**, *28*, 4623–4629. (b) Fernández, E. J.; Jones, P. G.; Laguna, A.; López-de-Luzuriaga, J. M.; Monge, M.; Pérez, J.; Olmos, M. E. *Inorg. Chem.* **2002**, *41*, 1056–1063.

(39) Cheng, Y.-D.; Zhang, L.-Y.; Qin, Y.-H.; Cheng, Z.-N. *Inorg. Chem.* **2005**, *44*, 6456–6462.

(40) Heyduk, A. F.; Krodel, D. J.; Meyer, E. E.; Nocera, D. G. *Inorg. Chem.* **2002**, *41*, 634–636.

(41) (a) Balch, A. L.; Catalano, V. J. *Inorg. Chem.* **1992**, *31*, 3934–3942. (b) Balch, A. L.; Guimerans, R. R.; Linehan, J.; Olmstead, M. M.; Oram, D. E. *Organometallics* **1985**, *4*, 1445–1451.

(42) (a) Forniés-Cámer, J.; Masdeu-Bultó, A. M.; Claver, C.; Tejel, C.; Ciriano, M. A.; Cardin, C. J. *Organometallics* **2002**, *21*, 2609–2618. (b) Farr, J. P.; Olmsteak, M. M.; Balch, A. L. *J. Am. Chem. Soc.* **1980**, *102*, 6654–6656.

(43) Forniés, J.; Ibáñez, S.; Martín, A.; Gil, B.; Lalinde, E.; Moreno, M. T. *Organometallics* **2004**, *23*, 3963–3975.

(44) Mealli, C.; Pichierri, F.; Randaccio, L.; Zangrando, E.; Krumm, M.; Holtenrich, D.; Lippert, B. *Inorg. Chem.* **1995**, *34*, 3418–3424.

(45) (a) Balch, A. L.; Catalano, V. J. *Inorg. Chem.* **1992**, *31*, 2569–2575. (b) Tanase, T.; Toda, H.; Kobayashi, K.; Yamamoto, Y. *Organometallics* **1996**, *15*, 5272–5274.

(46) (a) Forniés, J.; García, A.; Lalinde, E.; Moreno, M. T. *Inorg. Chem.* **2008**, *47*, 3651–3660. (b) Stork, J. R.; Olmstead, M. M.; Fettinger, J. C.; Balch, A. L. *Inorg. Chem.* **2006**, *45*, 849–857. (c) Balch, A. L.; Rowley, S. P. *J. Am. Chem. Soc.* **1990**, *112*, 6139–6140.

(47) Xu, X.; Fang, L.; Chen, Z.-X.; Yang, G.-C.; Sun, S.-L.; Su, Z.-M. *J. Organomet. Chem.* **2006**, *691*, 1927–1933.

(48) (a) Casida, M. E.; Jamorski, C.; Casida, K. C.; Salahub, D. R. *J. Chem. Phys.* **1998**, *108*, 4439–4449. (b) Statmann, R. E.; Scuseria, G. E. *J. Chem. Phys.* **1998**, *109*, 8218–8224. (c) Bauernschmitt, R.; Ahlrichs, R. *Chem. Phys. Lett.* **1996**, *256*, 454–464.

(49) (a) Tsipis, A. C.; Stalikas, A. V. *New J. Chem.* **2007**, *31*, 852–859. (b) Kosa, M.; Karni, M.; Apeloig, Y. *Organometallics* **2007**, *26*, 2806–2814. (c) Novozhilova, I. V.; Volkov, A. V.; Coppens, P. *Inorg. Chem.* **2004**, *43*, 2299–2307.

(50) (a) Pan, Q.-J.; Fu, H.-G.; Yu, H.-T.; Zhang, H.-X. *Inorg. Chem.* **2006**, *45*, 8729–8735. (b) Pan, Q.-J.; Zhang, H.-X.; Zhou, X.; Fu, H.-G.; Yu, H.-T. *J. Phys. Chem. A* **2007**, *111*, 287–294.

(51) (a) Pan, Q.-J.; Zhou, X.; Zhang, H.-X.; Fu, H.-G. *Chem. Phys. Lett.* **2008**, *453*, 7–12. (b) Liu, T.; Zhou, X.; Zhang, H.-X.; Xia, B.-H. *Dalton Trans.* **2008**, *1065*, 1072.

(52) (a) Bowmaker, B. A.; Schmidbaur, H.; Krüger, S.; Rösch, N. *Inorg. Chem.* **1997**, *36*, 1754–1757. (b) Häberlen, O. D.; Rösch, N. *J. Phys. Chem.* **1993**, *97*, 4970–4973.

(53) Møller, C.; Plesset, M. S. *Phys. Rev.* **1934**, *46*, 618–622.

(54) (a) Wadt, W. R.; Hay, P. J. *J. Chem. Phys.* **1985**, *82*, 284–298. (b) Hay, P. J.; Wadt, W. R. *J. Chem. Phys.* **1985**, *82*, 299–310.

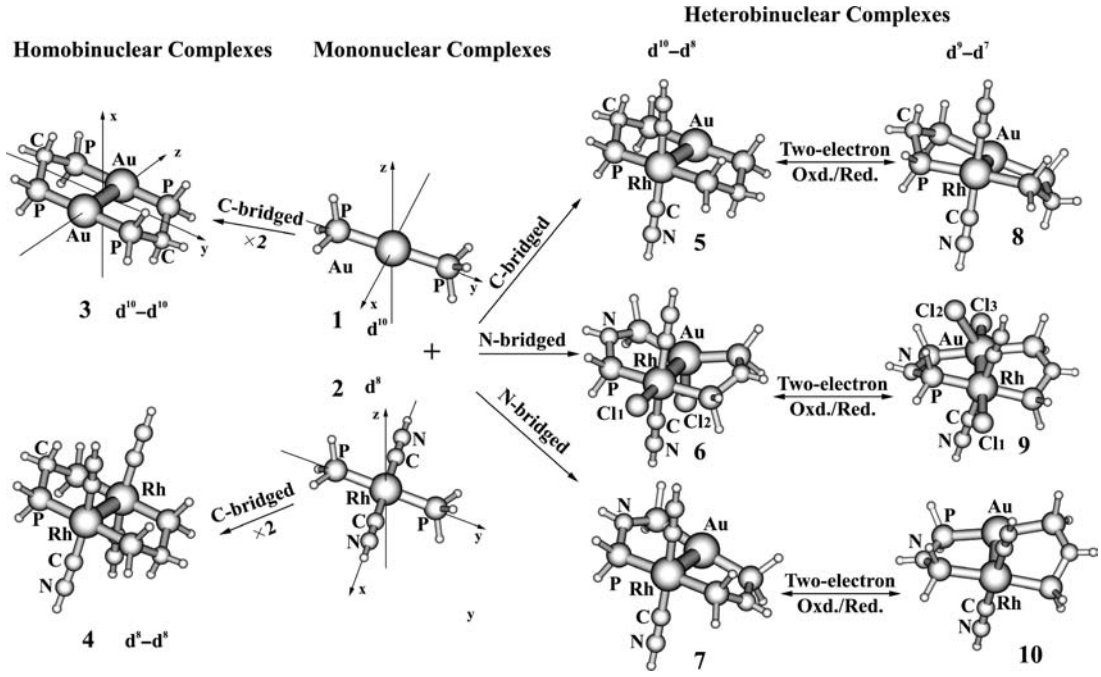

Figure 1. The structures of **1**−**10** associated with the depicted coordinate orientation.

Table 1. Optimized Geometry Parameters of **1**−**10** in the Ground States Using the MP2 Method, Together with the Experimental Values from X-Ray Diffraction[a] (distances in angstroms and angles in degrees)

	1	**2**	**3**		**4**	**5**		**6**		**7**	**8**	**9**		**10**
parameters	^1A_g	^1A_g	^1A_g	exptl.	^1A_g	^1A	exptl.	^1A	exptl.	^1A	^1A	^1A	exptl.	^1A
M−M′			3.024	2.939	2.945	2.890	2.921	2.758	2.818	2.808	2.566	2.590	2.655	2.546
Au−P	2.379		2.379	2.319		2.371	2.315	2.365	2.273	2.365	2.460	2.351	2.301	2.455
Rh−P		2.340			2.326	2.336	2.319	2.292	2.288	2.327	2.457	2.335	2.305	2.443
Rh−C		1.945			1.934	1.947	1.956	1.926	1.982	1.951	2.018	1.960	1.993	2.020
Rh−Cl1								2.471	2.603			2.442	2.376	
Au−Cl2								2.569	2.663			2.691	2.849	
Au−Cl3												2.408	2.427	
C≡N		1.180			1.182	1.179	1.170	1.182	1.149	1.178	1.173	1.176	1.145	1.172
P···P			3.078		3.048	3.055		3.028		3.037	3.001	2.972		2.979
P−Au−P	180.0		178.7	173.9		174.2	175.0	148.3	151.4	172.2	169.6	170.6	174.6	172.5
P−Rh−P		180.0			177.5	177.9	173.0	172.9	166.5	178.4	172.3	174.5	174.6	175.6
C−Rh−C		180.0			164.0	171.6		164.6	175.4	173.5	176.6	178.9	175.7	175.9
P−M−M′−P			0.0		0.0	2.4		−17.9	−14.8	11.6	12.5	−26.3	−22.4	−23.9

[a] Experimental values from refs 7, 8a, 8b, 28, and 29.

and P ($\alpha_d = 0.34$).[11] All calculations were accomplished using the Gaussian 03 program package.[55]

3. Results and Discussion

3.1. Ground States. 3.1.1. Geometry Structures. The optimized geometry structures of **1**−**10** are presented in Figure 1. Selected results from the geometry optimizations are summarized in Table 1 and compared to available experimental values.[7,8a,b,28,29] More detailed information is given in S-Table 4 (Supporting Information). Complex **1** has a typical linear two-coordinated geometry, and **2** exhibits a square-planar tetra-coordination (Figure 1). Similar cases were found for binuclear **3**−**7**. These geometry features are quantitatively reflected in Table 1. If isoelectronic CH_2 and NH groups are used to bridge **1** and **2**, binuclear complexes form, including the homobimetallic C-bridged **3** and **4**; heterobimetallic C-bridged **5** and **8**; and heterobimetallic N-bridged **6**, **7**, **9**, and **10** (Figure 1).

Homobimetallic **3** and **4** and heterobimetallic **5** with the CH_2 bridgehead display an approximately eclipsed P−M−P geometry arrangement. This can be proved by the calculated P−M−M′−P dihedrals of 0.0°, 0.0°, and 2.4°, respectively, for these complexes. In contrast, heterobimetallic **6** with the NH group forms a staggered conformation with a P−Au−Rh−P dihedral of −17.9°, which agrees with the experimental value of −14.8°.[29] However, it is difficult to differentiate the influence of the CH_2/NH bridgehead on the molecular structures by comparing **5** with **6**, with the existing bonding M−Cl interaction in **6**. Therefore, we optimized a theoretical model for **7** with free Cl ions. Its P−Au−Rh−P dihedral was calculated to be 11.6°. Therefore, we can simply deduce that CH_2-bridging diphosphine ligands tend to hold the MM′P_4 in a nearly eclipsed arrangement, especially for the homobinuclear complexes, while NH-bridging diphosphine ligands favor the staggered conformation. In addition, we note that another influence factor, the real complex $[Au^IRh^I(CN^tBu)_2(P(OCH_2CF_3)_2NMeP(OCH_2CF_3)_2)_2Cl_2]$, has some P−Au−Rh−P dihedral torsion; its bulk ligands contribute to the dihedral torsion.

Weak metal−metal interaction in binuclear complexes has attracted much attention because it not only determines the photophysical and photochemical properties of complexes but also plays an important role in biological systems.[56] The Au(I)−Au(I) distance in **3** was calculated at 3.024 Å (Table 1), falling within the range of 2.8−3.2 Å reported in experiments.[1−9] We predicted the Rh(I)−Rh(I) distance for **4** to be 2.945 Å, which is shorter than reported values of 3.239 Å for $[Rh_2(CO)_2Cl_2(PPh_2CH_2PPh_2)_2]$,[14a] 3.396 Å for $[Rh_2(CO)_2Cl_2(AsPh_2CH_2AsPh_2)_2]$,[14b] 3.037 Å for $[Rh_2(dmb)_2(PPh_2CH_2PPh_2)_2]\cdot(BPh_4)_2$,[14c] 3.070 Å for $[Rh_2(\mu\text{-}HTP5)_2(PPh_2CH_2PPh_2)_2]\cdot(BPh_4)_2$ (HTP5 = 1,5-diisocyano-1,1,5-triphenylpentane),[14d] 3.151 Å for $[Rh_2(dimen)_2(PPh_2CH_2PPh_2)_2]\cdot(BPh_4)_2$ (dimen = 1,8-diisocyanomenthane),[14e] 3.233 Å for $[Rh_2(dmb)_4]\cdot(BPh_4)_2$ (dmb = 2,2-dimethyl-1,3-diisocyanopropane),[14c] 3.242 Å for $[Rh_2(diprop)_4]^{2+}$,[14f,g] 3.193 Å for $[Rh_2(CNPh)_8]\cdot(BPh_4)_2$,[17b] and 3.287 Å for $[Rh_2(CNC_6H_{11})_8]\cdot(BF_4)_2$.[17] With respect to heterobimetallic complexes **5**, **6**, and **7**, the Au(I)−Rh(I) separations were estimated to be 2.890, 2.758, and 2.808 Å, respectively. The former two are comparable to the experimental values of 2.921 and 2.818 Å, respectively.[28,29] The calculated heterobimetallic distances (2.758−2.890 Å) are shorter than the corresponding homobimetallic analogs (2.945−3.024 Å). On the one hand, this is caused by the geometry arrangement: the staggered structure in heterobimetallic complexes facilitates gold−rhodium approaching each other, even if **5** only has a small P−Au−Rh−P dihedral of 2.4°. On the other hand, the MP2 greatly overestimates the hetero metal−metal interaction indicated in the literature.[6a,51]

Binuclear complexes **3**−**7** with closed-shell electronic structures share commonalities: the calculated M−M′ distances are slightly shorter than the van der Waals contacts;[57] the bite distances of P···P are apparently longer than corresponding M−M′ separations; and the P−M−M′ and P−M′−M angles have been calculated to be more than right angles (the calculated P−Rh−Au angle of 85.7° for **6** mainly results from Cl atom perturbations, proving that the angle was predicted to be 93.8° for **7** without the Cl atoms). These results suggest that the weak bonding interaction possibly occurs between the two metal centers. To estimate the interaction, we have carried out frequency calculations on the complexes at the MP2 level. The frequencies at 91, 130, 127, 134, and 143 cm^{-1} were attributed to M−M′ stretching vibrations for **3**−**7**, respectively, which are comparable to our previous results.[6,12,50,51] Herein, the calculated value of **3** is comparable to a resonance-enhanced band at 88 cm^{-1} from the resonance Raman spectra for $[Au_2(PCy_2CH_2PCy_2)_2]\cdot(ClO_4)_2$.[8a] However, the Rh−Rh stretching vibration frequency of 130 cm^{-1} for **4** is far stronger than the reported value of 85 cm^{-1} for $[Rh_2(diprop)_4]^{2+}$.[15] This is related to the much longer Rh−Rh distance (3.242 Å) found in $[Rh_2(diprop)_4]^{2+}$.[14f,g] Additionally, these calculated results show that the vibration frequencies of Au−Rh and Rh−Rh range from 127 to 143 cm^{-1}, which are higher than thos efor Au−Au, Au−Pt, and Pt−Pt. We attribute this to the lower mass of rhodium. In brief, the present calculated results, together with experimental reports, predict the existence of weak metal−metal bonding interaction in these binuclear gold and rhodium complexes.

As the literature states,[28−31] the Au(I)−Rh(I) complexes **5**−**7** have so-called d^{10}−d^8 metal-centered electronic configurations. The two-electron oxidization results in the formation of the Au(II)−Rh(II) complexes **8**−**10**. In these d^9−d^7 systems, the Au−Rh covalent bond can be formed by a single electron from the metal centers. Therefore, the Au(II)−Rh(II) distances were estimated to be 2.566, 2.590, and 2.546 Å for **8**, **9**, and **10**, respectively, and are much shorter than those of **5**−**7**. Correspondingly, the calculated metal−metal stretching vibrational frequencies are greatly enhanced to 212, 183, and 222 cm^{-1}.

Optimizations on these gold and rhodium complexes, **1**−**10**, indicate that the agreement between the calculated results and experimental values is very good in some cases. As stated in the literature,[11] this excellent agreement should be attributed to a cancelation of errors. On one hand, MP2 tends to overestimate the weak metal−metal interaction, but this effect is counterbalanced by the incompleteness of the basis sets. On the other hand, the substituent approximation, replacing the real methyl, phenyl, and other heavy groups with the hydrogen atom, will affect the calculated results.

3.1.2. Electronic Structures. 3.1.2.1. Mononuclear Complexes. In S-Tables 5−14 (Supporting Information), we summarize the electronic structures for **1**−**10**. The coordinate orientation is depicted in Figure 1. The occupied orbitals of **1** have significant Au characters. $10a_g$ (highest occupied molecular orbital, HOMO) is composed of 31.2% s(Au), 12.8% d_{z^2}(Au), and 38.5% $d_{z^2-x^2}$(Au). The next lower-energy $7a_u$ molecular orbital (MO) has the Au−P σ bonding character. The combination of d_{z^2} and $d_{z^2-x^2}$ contributes to the $9a_g$ orbital making up most of the d_{z^2} composition (65.7%). The lower-energy unoccupied orbitals mainly come from Au 6p contributions. For the mononuclear d^8 complex **2**, the Rh 4d is the predominant contribution to the higher-energy occupied orbitals, with some participation from the CNH group. $12a_g$ (HOMO), $4b_g$, $3b_g$, and $11a_g$ MOs are main-

(55) Frisch, M. J.; Trucks, G. W.; Schlegel, H. B.; Scuseria, G. E.; Robb, M. A.; Cheeseman, J. R.; Montgomery, J. A., Jr.; Vreven, T.; Kudin, K. N.; Burant, J. C.; Millam, J. M.; Iyengar, S. S.; Tomasi, J.; Barone, V.; Mennucci, B.; Cossi, M.; Scalmani, G.; Rega, N.; Peterson, G. A.; Nakatsuji, H.; Hada, M.; Ehara, M.; Toyota, K.; Fukuda, R.; Hasegawa, J.; Ishida, M.; Nakajima, T.; Honda, Y.; Kitao, O.; Nakai, H.; Klene, M.; Li, X.; Knox, J. E.; Hratchian, H. P.; Cross, J. B.; Adamo, C.; Jaramillo, J.; Gomperts, R.; Stratmann, R. E.; Yazyev, O.; Austin, A. J. ; Cammi, R.; Pomelli, C.; Ochterski, J. W.; Ayala, P. Y.; Morokuma, K.; Voth, G. A.; Salvador, P.; Dannenberg, J. J.; Zakrzewski, V. G.; Dapprich, S.; Daniels, A. D.; Strain, M. C.; Farkas, O.; Malick, D. K.; Rabuck, A. D.; Raghavachari, K.; Foresman, J. B.; Ortiz, J. V.; Cui, Q.; Baboul, A. G.; Clifford, S.; Cioslowski, J.; Stefanov, B. B.; Liu, G.; Liashenko, A.; Piskorz, P.; Komaromi, I.; Martin, R. L.; Fox, D. J.; Keith, T.; Al-Laham, M. A.; Peng, C. Y.; Nanayakkara, A.; Challacombe, M.; Gill, P. M. W.; Johnson, B.; Chen, W.; Wong, M. W.; Gonzalez, C.; Pople, J. A. *Gaussian 03*, revision B.03; Gaussian, Inc.: Pittsburgh, PA, 2003.

(56) (a) Blackburn, N. J.; Barr, M. E.; Woodruff, W. H.; van der Ooost, J.; de Vries, S. *Biochemistry* **1994**, *33*, 10401–10407. (b) Barabasz, W.; Hetmańska, B.; Tomasik, P. *Water, Air, Soil Pollut.* **1990**, *52*, 337–357. (c) Bogusława, H.; Tomasik, P.; Tuszyński, T. *Water, Air, Soil Pollut.* **1994**, *74*, 281–288. (d) Beri, R.; Kumar, V.; Chandra, R. *Biochem. Soc. Trans.* **1992**, *20*, 354S.

(57) (a) Bondi, A. *J. Phys. Chem.* **1964**, *68*, 441–451. (b) Slater, J. C. *J. Chem. Phys.* **1964**, *41*, 3199–3204.

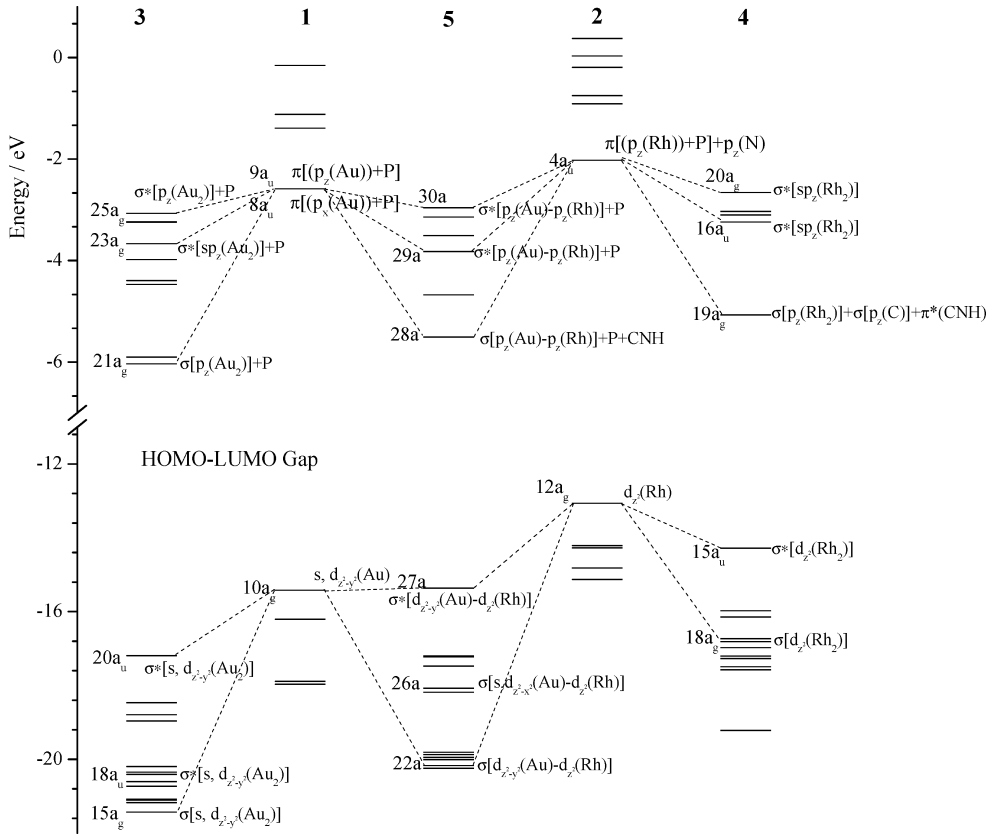

Figure 2. Energy-level diagrams of the frontier molecular orbitals for mononuclear $[Au^I(PH_3)_2]^+$ (**1**) and $[Rh^I(CNH)_2(PH_3)_2]^+$ (**2**), homobinuclear $[Au^I_2(PH_2CH_2PH_2)_2]^{2+}$ (**3**) and $[Rh^I_2(CNH)_4(PH_2CH_2PH_2)_2]^{2+}$ (**4**), and heterobinuclear $[Au^IRh^I(CNH)_2(PH_2CH_2PH_2)_2]^{2+}$ (**5**).

ly formed by Rh 4d components with 83.1% d_{z^2}, 85.1% d_{xz}, 93.1% d_{yz}, and 81.6% d_{xy}, respectively. Similar to the mononuclear d^{10} complex **1**, the lower-energy unoccupied MOs of **2** mainly come from the Rh 5p contributions. The p_z(Rh) combined with some p_z(CNH) and p_z(P) characteristics forms the lowest unoccupied molecular orbital (LUMO; $4a_u$) with π[Rh−P−C] + π*[CNH]. This agrees with a previous proposal that the π-acceptor d^8 complexes have empty orbitals with the admixture of metal $(n + 1)p_z$ and ligand-based π characters.[18]

3.1.2.2. Interaction to Raise Binuclear Complexes from Mononuclear Complexes. In terms of geometry structure, homobinuclear **3** and **4** and heterobinuclear **5**−**7** can simply be fabricated from d^{10} (**1**) and d^8 (**2**) monomers. Complexes **3**, **4**, and **5** employ the CH_2 bridgehead in the diphosphine ligand, and **6** and **7** take the isoelectronic NH bridgehead. We describe the electronic structures of C-bridged **3**−**5** dimers and the **1** and **2** monomers in Figure 2. Apparently, the metal−metal interaction strongly modifies the original orbitals of the monomers. Most orbitals of binuclear complexes have lower energy relative to those of mononuclear complexes. Two original atomic orbitals (AOs) interact and split into two MOs. For example, the interaction of the d_{xy}(Rh) AOs of **4** (S-Table 8, Supporting Information) forms δ and δ* bonds in $17a_g$ and $14a_u$ MOs, respectively. The π orbitals come from d_{xz}(Rh) and d_{yz}(Rh) AOs to give d_{xz} π ($17b_u$) and π* ($15b_g$) as well as d_{yz} π ($16b_u$) and π* ($14b_g$) orbitals. For the two metal−metal σ and σ* orbitals, $18a_g$ and $15a_u$ (HOMO) are mainly composed of d_{z^2}(Rh) AOs. For lower-energy unoccupied orbitals, the p_z(Rh) interactions give rise to the σ ($19a_g$), σ* ($16a_u$), and σ* ($20a_g$), where there is significant s contribution to the latter two orbitals.

Similar to homobinuclear **3** and **4**, the metal−metal interaction in heterobinuclear **5** rectifies the original AOs of monomers. However, the difference between gold and rhodium atoms in electronic properties determines their contributions to MOs. For instance, the HOMOs of **1** and **2** interact to form the σ*(Au−Rh) (27a, HOMO) and σ(Au−Rh) (22a) of **5**. Rhodium and gold contribute 60.0% and 25.6%, respectively, to the HOMO, with d_{z^2}(Rh) providing the biggest contribution at 55.1% (S-Table 9, Supporting Information). Consequently, the HOMO of **2** has a large decrease in energy, and the HOMO of **1** slightly changes (Figure 2). The LUMO of **5** exhibits σ(Au−Rh) characters with 14.7% p_z(Au) and 16.7% p_z(Rh) components. The ligands of PH_2, CH_2, and CNH account for about 25.4%, 23.4%, and 14.3%, respectively. Therefore, the ligands play an indispensable role in the electronic transitions.

In hydrogen production, Nocera et al.[27−29] found that overall it is advantageous to activate the Rh−X bond in bimetallic rhodium complexes and their derivatives. One way to increase the photocycle efficiency is to increase the photochemical quantum yield for Rh−X bond activation. Therefore, the nature of the metal−halide bond and strategies to activate the bond are a major focus of current research. Our calculations on the halide complex **6** demonstrate significant Cl participation in its higher-energy occupied orbitals (S-Table 10, Supporting Information). The HOMO

Table 2. Calculated Absorptions of $[Au^{I}Rh^{I}(CNH)_2(PH_2CH_2PH_2)_2]^{2+}$ (**5**) in Acetonitrile at the TD-DFT(B3LYP)/C-PCM level, Associated with the Absorptions Observed in the Experiment

						exptl.[a]	
states	conf.	|CI coeff.| > 0.2	λ (nm)	E (eV)	f	$Y^- = PF_6^-$	ClO_4^-
^3A	27a → 28a	0.73753	518.81	2.3898	0.0000	546 (150)	525 (600)
^1A	27a → 28a	0.69103	455.44	2.7223	0.3260	455 (19000)	455 (24000)
^1A	27a → 29a	0.65211	335.70	3.6933	0.0007	381 (sh)	
^1B	26b → 28a	0.69807	329.01	3.7684	0.0535	340 (7500)	342 (9440)
^1B	27a → 27b	0.70211	314.31	3.9446	0.0172		
^1B	25b → 28a	0.68762	309.64	4.0042	0.1247	312 (sh)	
^1B	27a → 28b	0.70252	288.30	4.3005	0.0010		
^1A	27a → 30a	0.66332	268.80	4.6124	0.0602		
^1B	26b → 29a	0.64520	267.16	4.6408	0.0054		

[a] The experimental absorption spectra of $[Au^{I}Rh^{I}(CN^{t}Bu)_2(PPh_2CH_2PPh_2)_2]^{2+}\cdot(Y^-)_2$ ($Y^- = PF_6^-$ and ClO_4^-) from ref 30.

has σ*(Au−Rh) and σ(Rh−Cl) characters. The next five occupied orbitals mainly exhibit π(Cl) character. However, there is nearly no Cl contribution to the LUMO at less than 2%. The electronic density mainly focuses around the ion $[Au^{I}Rh^{I}(CNH)_2(PH_2NHPH_2)_2]^{2+}$. Upon excitation into the LUMO, the transfer from the Cl to the ion occurs, which might promote the M−X bond activation.

As stated in the literature,[7,13−16,28−31] **3**, **4**, and **5** have quasi $d^{10}-d^{10}$, d^8-d^8, and $d^{10}-d^8$ electronic structures, respectively. However, the relativistic effects of heavy metals[58] causes the dispersion of some electrons into original empty metal (n + 1)s and (n + 1)p orbitals and results in a weak metal−metal bonding. This is reflected in the calculated M−M′ bond orders of **3**−**7**: 0.019, 0.017, 0.023, 0.063, and 0.027, respectively.

3.1.2.3. Two-Electron Oxidized Derivatives. As mentioned above, the two-electron oxidations in **8**−**10** have different geometry features from those of **5**−**7**. For example, the Au−Rh separations in the former are much shorter. Complex **5** possesses most of the Au and Rh contributions in the frontier molecular orbitals, such as the HOMO of σ*[$d_{z^2-y^2}$(Au)−d_{z^2}(Rh)] and the LUMO of σ[p_z(Au)−p_z(Rh)], as seen in S-Figure 2 and the S-Tables (Supporting Information). The complex has a quasi-bimetallic $d^{10}-d^8$ structure. During oxidation, two electrons in the original HOMO (σ*) of **5** are removed. So, **8** displays the HOMO of σ(Au−P) + σ(Rh−P) and a LUMO of σ*[$d_{z^2-y^2}$(Au)−d_{z^2}(Rh)]. Consequently, the Au−Rh distances are greatly shortened in **8** relative to that in **5**. Similar cases occur in **6** and **9** as well as **7** and **10**. The Au−Rh bond orders of **8**−**10** were calculated to be 0.604, 0.616, and 0.612, respectively, far exceeding those of **5**−**7**.

3.2. Electronic Spectra. 3.2.1. Mononuclear Complexes. S-Table 15 (Supporting Information) shows that **1** has the lowest-energy absorption band at 202 nm (6.12 eV). This is caused by the combination of the $10a_g \rightarrow 8a_u$ (HOMO → LUMO) and $10a_g \rightarrow 9a_u$ (HOMO → LUMO + 1) configurations. According to S-Table 16 (Supporting Information), the absorption band can be attributed to the $d_{z^2-y^2}$(Au) → p_z(Au)/p_x(Au) (metal-centered, MC) transition. We also obtained some low-lying d → p absorptions. Under C_i symmetry, they have combined d orbital characteristics. With respect to mononuclear **2** under C_{2h} symmetry, three low-lying d → p

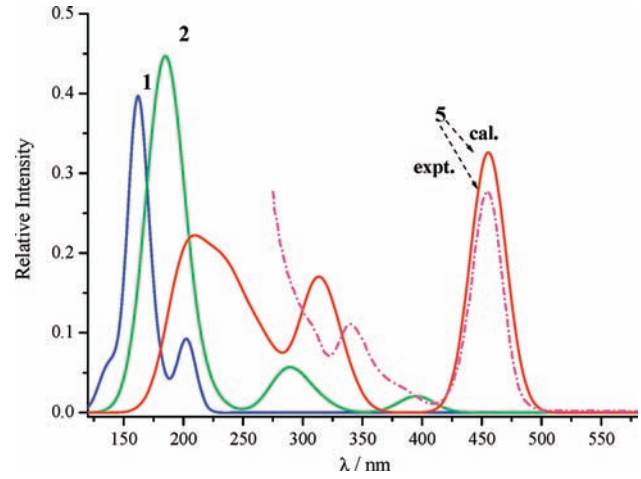

Figure 3. Simulated absorption spectra in acetonitrile for mononuclear **1** and **2** as well as heterobinuclear **5** from the TD-DFT(B3LYP)/C-PCM calculations, together with experimental spectra of $[Au^{I}Rh^{I}(CN^{t}Bu)_2(PPh_2CH_2PPh_2)_2]\cdot(PF_6)_2$.

absorptions in acetonitrile were calculated at 395, 311, and 287 nm, corresponding to d_{z^2}(Rh) → π[p_z(Rh−P−C)] + π*[p_z(CNH)], d_{yz}(Rh) → π[p_z(Rh−P−C)] + π*[p_z(CNH)], and d_{xz}(Rh) → π[p_z(Rh−P−C)] + π*[p_z(CNH)] transitions, respectively. The absorptions are comparable to experimental values of 400, 350, and 317 nm.[13b]

3.2.2. Binuclear Complexes. The experimental measurements were reproduced well by the theoretical transitions (calculated results of **3** come from ref 12b). The theoretical spectrum of **4** contains two strong peaks at 604 nm (2.05 eV) and 299 nm (4.15 eV; S-Figure 4a, Supporting Information). The 604 nm lowest-energy absorption has the largest oscillator strength (0.320). It comes from the $15a_u \rightarrow 19a_g$ (HOMO → LUMO) configuration, attributed to a σ*[d_{z^2}(Rh_2)] → σ[p_z(Rh_2)] + π*(CNH) + P transition (S-Tables 19 and 20, Supporting Information). We related it to experimental 606, 573, 521, and 559 nm absorptions for $[Rh_2(CNR)_4(PPh_2CH_2PPh_2)_2]\cdot(PF_6)_2$ (R = Ph, Me, ^{t}Bu, and ^{n}Bu) in acetonitrile at room temperature.[13] The calculated 299 and 292 nm absorptions have admixtures of π[d_{xz}(Rh_2)] + π[d_{yz}(Rh_2)] → σ[p_z(Rh_2)] + π*(CNH) + P transitions corresponding to the higher-energy absorption peak in the experiment.

Similarly, the calculated results of **5** agree well with experimental reports, as seen in Table 2 and Figure 3. The lowest-energy spin-allowed absorption was predicted at 455 nm. It was assigned as a σ*[d_{z^2}(Rh)−$d_{z^2-y^2}$(Au)] →

(58) Pyykkö, P. *Chem. Rev.* **1988**, *88*, 563–594.

Table 3. Partial Molecular Orbital Contributions (%) of $[Au^{I}Rh^{I}(CNH)_2(PH_2CH_2PH_2)_2]^{2+}$ (**5**) in Acetonitrile under the TD-DFT(B3LYP)/C-PCM Calculations

		contributions (%)							
orbitals	energy (eV)	Au	Rh	$4PH_2$	$2CH_2$	2CNH	Au components (%)	Rh components (%)	ligand components (%)
30a	−0.5513	27.4	21.0	40.0	6.7	4.8	10.2s 13.2p_z 2.7$d_{z^2-x^2}$	17.4s 2.8$d_{x^2-y^2}$	13.5s(P_{Au}) 2.3p_y(P_{Au})
28b	−0.6691	0.7	7.2	30.1	8.5	53.6		6.7p_y	11.9s(P_{Rh}) 13.8p_y(C) 12.7p_y(N)
29a	−0.9510	6.1	26.4	46.3	6.2	15.0	3.3s 2.2p_z	5.6s 19.8$d_{x^2-y^2}$	2.2s(P_{Au}) 14.4s(P_{Rh}) 5.5p_y(P_{Rh}) 4.5s(C)
27b	−1.1399	34.6	3.4	47.3	11.7	2.9	34.2p_x	2.1d_{xz}	6.8p_x(P_{Au})
28a	−2.3435	15.8	16.6	24.3	17.0	26.4	3.6s 9.9p_z	14.2p_z	2.6s(P_{Au}) 2.4p_y(P_{Au}) 2.0p_z(P_{Rh}) 4.8p_z(C) 8.0p_z(N)
							HOMO−LUMO Gap		
27a	−6.0162	21.0	68.1	7.0	0.5	3.4	4.5p_z 12.0d_{z^2} 2.6$d_{z^2-x^2}$	4.6s 2.0p_z 61.5d_{z^2}	
26b	−7.2122	5.3	85.5	4.0	5.0	0.3	5.2d_{yz}	84.7d_{yz}	
25b	−7.3172	6.6	76.9	0.2	0.1	16.1	6.3d_{xz}	76.3d_{xz}	7.1p_z(N)
26a	−8.1355	0.7	77.9	1.5	3.4	16.5		76.9d_{xy}	8.1p_y(N)

$\sigma[p_z(Au-Rh)] + \pi^*(CNH) + P$ transition. As shown in Table 3, the σ^* orbital receives contribution mainly from d_{z^2}(Rh) (61.5%). Furthermore, the absorption should include three contributions: $\sigma^*(d) \rightarrow \sigma(i)$ (MC transition), $\sigma^*(d) \rightarrow$ ligand (metal to ligand charge transfer, MLCT), and $d_{z^2}(Rh) \rightarrow p_z(Au)$ (metal to metal charge transfer, MMCT). The first two transitions were found in homobinuclear complexes **3** and **4**. The third is a unique characteristic for heterobinuclear complexes. We conjecture that MMCT may play an important role in producing weak metal−metal bonding interaction. The next absorption peak of **5** was predicted at 329 nm with $d_{yz}(Rh) \rightarrow \sigma[p_z(Au-Rh)] + \pi^*$ (CNH) + P transition properties. As a heavy metal element, the spin−orbit coupling of the Au and Rh atoms should be large; thus, the singlet-to-triplet transition may appear as weak tails in the absorption spectra. We predicted the spin-forbidden absorption to be at 519 nm (2.39 eV), having the same transition character as the spin-allowed 455 nm. $[Au^{I}Rh^{I}(CN^{t}Bu)_2(PPh_2CH_2PPh_2)_2]^{2+}\cdot(Y^-)_2$ ($Y^- = ClO_4^-$ and PF_6^-) has been observed to exhibit very weak absorptions at 525 and 546 nm.[30]

Nocera et al. found that the N-bridged complex $[Au^{I}Rh^{I}(CN^{t}Bu)_2(PR_2NMePR_2)_2Cl_2]$ ($R = OCH_2CF_3$) in the acetonitrile solution displays absorption bands at 419, 380, and 307 nm.[29] The lowest-energy band was experimentally attributed to a $\sigma^*(Rh-Au) \rightarrow \sigma(Au-Rh) + \pi^*(CN^{t}Bu)$ transition. After further oxidization, $[Au^{II}Rh^{II}(CN^{t}Bu)_2(PR_2NMePR_2)_2Cl_3]^+$ is formed with two new absorption bands at 460 and 329 nm.[29] For our study, we used the theoretical models for **6** and **9** to replace such real complexes. The general spectral pattern of the experimental spectra was reproduced well by the calculated results, as shown in S-Figures 5 and 6 (Supporting Information). We related the experimental absorption bands of the Au(I)−Rh(I) complex to the 406, 366, and 301 nm absorptions of **6**, as seen in S-Tables 21 and 22 (Supporting Information). The electron density diagrams of orbitals involved in the lowest-energy absorption support the assignment of the MC/MMCT/MLCT transitions (S-Figure 7, Supporting Information). Calculations reveal that these three absorptions were mainly contributed to by the 61a → 62a, 61a → 63a, and 61a → 66a configurations, respectively. Configuration 61a (HOMO) has $\sigma^*(Au-Rh) + \sigma(Rh-Cl)$ characteristics and the LUMO from $\sigma(Au-Rh) + \sigma^*(Rh-Cl)$. The other unoccupied 63a and 66a have no Cl contribution. Their electronic density focuses around metal centers and ligands excluding Cl. Therefore, electronic transitions involving these unfilled orbitals may promote M−X bond activation. Note that the difference between the calculated results and experimental values is mainly caused by the approximation of the hydrogen atom replacing the OCH_2CF_3 group.

Upon two-electron oxidation, Au(II)−Rh(II) complex **9** is formed. The conversion process was determined by a UV−vis absorption spectrum. Slightly different from those of **6**, the higher-energy occupied orbitals of **9** including the HOMO all have contributions mostly from Cl. For example, the 452 nm absorption contributed by the 63a → 65a configuration is attributed to $\pi(Cl2) \rightarrow \sigma^*[d_{z^2}(Rh)-d_{z^2-y^2}(Au)]$, corresponding to an experimental value of 460 nm.[29] Additionally, the intense peak of the oxidized product at 329 nm in experiments is comparable to the calculated absorptions of **9** at 324−341 nm. These calculated absorption transitions all have contributions from the 59a → 65a configuration. S-Figure 7 (Supporting Information) indicates that the 329 nm band belongs to a $\sigma[d_{z^2}(Rh)-d_{z^2-y^2}(Au)] \rightarrow \sigma^*[d_{z^2}(Rh)-d_{z^2-y^2}(Au)]$ transition.

3.2.3. Influence of Metal−Metal Interaction in Binuclear Complexes on Electronic Spectra. As discussed above, the metal−metal interaction in dimers lowers the d → p transition compared with those in monomers. For example, we calculated the $d_{z^2} \rightarrow p_z$ transition absorptions of **1** and **2** to be at 202 and 395 nm, respectively. Accordingly, the $\sigma^*(d_{z^2}) \rightarrow \sigma(p_z)$ absorptions were estimated at 291 nm for Au(I)−Au(I) complex **3**, 604 nm for Rh(I)−Rh(I) complex **4**, and 455 nm for Au(I)−Rh(I) complex **5**. To intuitively understand the influence of metal−metal interaction on $d_{z^2} \rightarrow p_z$ absorption, in Figure 4 we depict electron density diagrams of orbitals involved in such absorption transitions. Apparently, strong $d_{z^2}-d_{z^2}$ and p_z-p_z interactions in dimers result in a large red shift of absorption wavelength with respect to monomers. Figure 2 provides a qualitative and semiquantitative explanation for this red shift. In dimers, the metal−metal interaction stabilizes the $\sigma(p_z)$ (LUMO) and $\sigma^*(d_{z^2})$ (HOMO) compared to that in monomers. There is lower energy in the LUMO than in the HOMO, as shown in Figure 2. For binuclear **3**, the stabilization energy of $\sigma(p_z)$ was estimated to be 3.45 eV, far larger that that of $\sigma^*(d_{z^2})$ with 1.77 eV relative to those of monuclear **1**. Similar cases can be found in **4** and

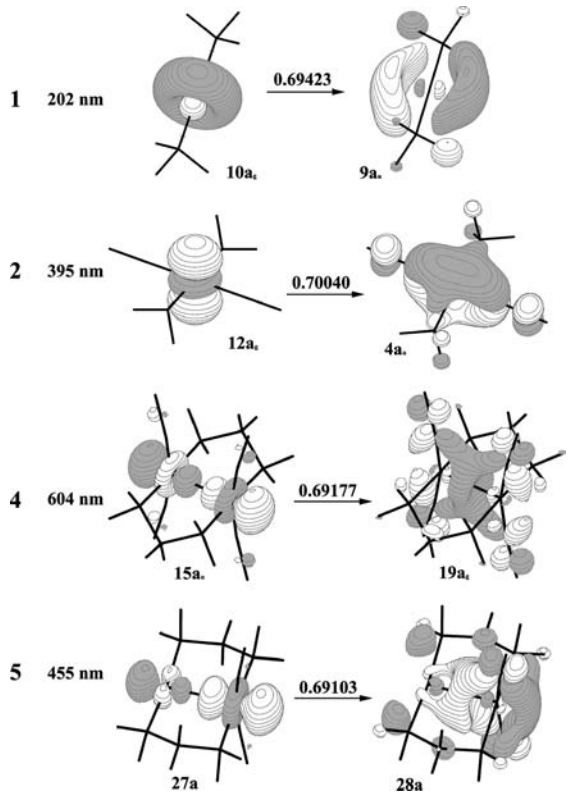

Figure 4. The single electron transitions with |CI coefficient| > 0.2 in the TD-DFT calculations for the $d_{z^2} \rightarrow p_z$ absorptions of **1**, **2**, **4**, and **5** in acetonitrile.

5. The $\sigma^*(d_{z^2}) \rightarrow \sigma(p_z)$ absorption band of **6** was predicted to be at 406 nm. There is only a small red shift of absorption wavelength relative to the 395 nm peak for **2**. In fact, this is closely correlated with the Cl atom participation in **6**. We can confirm this by calculating the electronic spectra of **7** excluding the Cl atoms. Indeed, the 489 nm $\sigma^*(d_{z^2}) \rightarrow \sigma(p_z)$ absorption is obtained at the B3LYP/C-PCM level.

3.3. Excited-State Properties. A theoretical understanding of the excited-state properties of binuclear gold and rhodium complexes serves as a foundation to developing their potential applications in photocatalysis and luminescent devices and to designing novel molecules. Here, the UMP2 optimized geometry parameters of **1**−**6** and **9** in triplet excited states are listed in Table 4.

Upon excitation, the geometry parameters of mononuclear **1** and **2** change slightly (Tables 1 and 4). These are correlated with the metal-localized $p_z \rightarrow d_{z^2}$ transitions (S-Figure 8, Supporting Information). In contrast, the metal-centered transition results in a large geometry change in binuclear **3**, **4**, and **5**. The UMP2 calculations for **4** predict that the Rh−Rh distance shrinks by about 0.24 Å in going from the ground state to the lowest-energy triple excited state, whereas the Rh−P bond lengths and the P···P bite distances remain nearly constant. It is apparent that the bonding interaction between the two Rh atoms drives the Rh−Rh shrinkage. Just like in **4**, similar changes were found for **3** and **5** during electronic excitation. Over the past two decades, many attempts have been made to predict the metal−metal distance in the triplet excited state through experiments and theoretical studies. For example, through Franck−Condon analysis,[59a,b] resonance Raman spectra,[59c] microsecond-resolved X-ray absorption fine structure,[59d] time-resolved X-ray diffraction,[60] and unrestricted theoretical methods,[50a,61] researchers summarized that the Pt−Pt distances of $Y_n[Pt^{II}_2(P_2O_5H_2)_4]$ ($Y = K^+$, $(n\text{-}Bu_4N)^+$, Ba^{2+}, and $(Et_4N)_3H^{4+}$) in the $^3[\sigma^*(d_{z^2})\sigma(p_z)]$ excited state contract an estimated 0.16−0.29 Å relative to the ground state. Similar predications were made for homobinuclear Au,[8a] Pt,[22a] and Rh[15c,d,62] and heterobinuclear Au−Pt[35a] complexes. Our present calculations agree with these results.

Analyses on the electronic structures reveal that the lowest-energy triplet excited states of homobinuclear **3** and **4** are produced by the promotion of electrons from the $\sigma^*(d_{z^2-y^2})$ and $\sigma^*(d_{z^2})$ antibonding orbitals to the $\sigma(p_z)$ bonding orbitals. During emission, the electron transfers from $\sigma(p_z)$ to $\sigma^*(d)$. Because their HOMOs have bonding characters, the metal−metal distances are strongly shortened. S-Figure 8 (Supporting Information) displays these processes in detail. It is worth noting that there exists an apparent $\sigma[p_z(C)-p_z(C)]$ interaction in the HOMO of **4**, which is responsible for the decrease of the C−Rh−Rh angle from 98.0° in the ground state to 92.9° in the excited state. In addition, the interaction contributes to the Rh−Rh contraction to some extent. Although the metal−metal contraction found in heterobinuclear **5** is similar to those in homobinuclear **3** and **4**, the difference of gold and rhodium results in unique electronic properties for the heterobinuclear complex. For homobinuclear complexes, the HOMOs and LUMOs are composed of 57.9% and 81.8% Au for **3** and 42.3% and 75.3% Rh for **4**, respectively. Even if we seriously consider the ligand-to-metal charge transfer (LMCT) transition, the $\sigma(p_z) \rightarrow \sigma^*(d_{z^2-y^2})/\sigma^*(d_{z^2})$ (MC) transition configuration still plays a predominant role in the emissive excited states. However, this is not the case in heterobinuclear complexes. Except for the MC and LMCT transitions in **5**, similar to those in **3** and **4**, the charge transfer between Au and Rh (MMCT) should be addressed.

$[Au_2(PR_2CH_2PR_2)_2]^{2+}$ (R = Me, Et, Cy and Ph), $[Rh_2(CNR)_4(PPh_2CH_2PPh_2)_2]^{2+}$ (R = Ph, Me, ^{t}Bu, and ^{n}Bu), and $[Au^IRh^I(CN^tBu)_2(PPh_2CH_2Ph_2)_2]^{2+}$ exhibit intense phosphorescent emissions in the ranges of 472−593, 572−610, and 769−952 nm, respectively.[7,8,13,30] In our present study, we attribute the emissive excited states to the MC/LMCT transitions for homobinuclear complexes and the MC/MMCT/LMCT transitions for heterobinuclear species. The assignments have modified previous theoretical[12,51] and experimental[7,8,13,30] reports and provided insight into the nature of the excited states for the binuclear complexes.

In the UMP2 calculations, **6** was predicted to have a low-lying ^{3}A triplet excited state. The Au−Rh distance shortens

(59) (a) Brummer, J. G.; Crosby, G. A. *Chem. Phys. Lett.* **1984**, *112*, 15–19. (b) Rice, S. F.; Gray, H. B. *J. Am. Chem. Soc.* **1983**, *105*, 4571–4575. (c) Leung, K. H.; Phillips, D. L.; Che, C.-M.; Miskowski, V. M. *J. Raman Spectrosc.* **1999**, *30*, 987–993. (d) Thiel, D. J.; Li¯vinš, P.; Stern, E. A.; Lewis, A. *Nature* **1993**, *362*, 40–43.
(60) Kim, C. D.; Pillet, S.; Wu, G.; Fullagar, W. K.; Coppens, P. *Acta Crystallogr.* **2002**, *A58*, 133–137.
(61) (a) Novozhilova, I. V.; Volkov, A. V.; Coppens, P. *J. Am. Chem. Soc.* **2003**, *125*, 1079. (b) Stoyanov, S. R.; Villegas, J. M.; Rillema, D. P. *J. Phys. Chem. B* **2004**, *108*, 12175.
(62) Novozhilova, I. V.; Volkov, A. V.; Coppens, P. *Inorg. Chem.* **2004**, *43*, 2299–2307.

Table 4. Optimized Geometry Parameters of **1**−**6** and **9** in the Triplet Excited States Using the UMP2 Method (distances in angstroms and angles in degrees)

parameters	**1** ^3A_u	**2** ^3A_u	**3** ^3A_u	**4** ^3A_u	**5** ^3A	**6** ^3A	**9** ^3A
M−M′			2.673	2.710	2.704	2.724	2.914
Au−P	2.375		2.406		2.370	2.331	2.408
Rh−P		2.366		2.344	2.372	2.318	2.340
Rh−C		1.963		1.942	1.960	1.930	1.969
Rh−Cl1						2.512	2.476
Au−Cl2						2.512	2.518
Au−Cl3							2.489
C≡N		1.182		1.183	1.179	1.181	1.176
P···P			3.084	3.060	3.077	2.933	3.027
P−Au−P	180.0		170.2		172.4	179.5	164.4
P−Rh−P				171.4	169.6	169.7	175.5
C−Rh−C				174.2	177.2	178.7	174.2
P−M−M′−P			0.0	0.0	−1.9	37.5	16.9

by about 0.03 Å in going from the ground state to the triplet excited state. For **9**, we presented a low-lying excited state with a Au−Rh distance of 2.914 Å, which is longer than the 2.590 Å for the ground state. S-Figure 9 (Supporting Information) details the Au−Rh changes upon excitation. Nocera et al.[29] determined that $[Au^{I}Rh^{I}(CN^{t}Bu)_2(PR_2NMePR_2)_2Cl_2]$ (R = OCH_2CF_3) and $[Au^{II}Rh^{II}(CN^{t}Bu)_2(PR_2NMePR_2)_2Cl_3]^+$ are emissive at 707 and 733 nm, respectively. We assigned these emissions to the $\pi[p_x(Au-P)] \rightarrow \sigma^*[d_{z^2-y^2}(Au)-d_{z^2}(Rh)]$ and $\sigma^*[d_{z^2-y^2}(Au)-d_{z^2}(Rh)] \rightarrow \sigma[d_{z^2-y^2}(Au)-d_{z^2}(Rh)]$ transitions, respectively.

In addition, we carried out frequency calculations on **3**−**6** and **9** for the lower-energy triplet excited states to characterize the metal−metal interactions. Because the HOMOs of **3**−**6** in their triplet excited states have bonding properties, the excited-state M−M′ stretching frequencies should be higher than those of the ground states. Through vibrational-mode analyses, the calculated 145, 200, 168, and 158 cm^{-1} frequencies of **3**−**6** in the excited states are attributed to the M−M′ stretching frequencies and, as expected, are much higher than the 91, 130, 127, and 134 cm^{-1} frequencies in the ground state, respectively. This suggests that the interaction between the two metal atoms is weak in the ground state but strongly enhanced in the triplet excited state. In contrast, the promotion of electrons into the σ^*(d) for **9** results in a lower excited-state frequency (137 cm^{-1}) than for the ground state (183 cm^{-1}). Our calculated results for **3**−**6** in the excited states are comparable to experimental values of 144 cm^{-1} for $\{[Au_2(PCy_2CH_2PCy_2)_2]\cdot(ClO_4)_2\}^*$,[8a] 150 cm^{-1} for $\{[Rh_2(diprop)_4]^{2+}\}^*$,[15] 145 cm^{-1} for *trans*-$[Pt_2(CN)_4(PCy_2H_2CPCy_2)_2]^*$,[22] 146 cm^{-1} for $\{[Pt_2(pcp)_4]^{4-}\}^*$,[21] and 155 cm^{-1} for $\{[Pt_2(pop)_4]^{4-}\}^*$[59,60] 181 cm^{-1} for $\{[AuPt(CN)_2(PCy_2CH_2PCy_2)_2]\cdot(ClO_4)\}^*$.[35a]

4. Conclusions

The ground and excited states of **1**−**10** were explored theoretically. In the ground state, the HOMOs and LUMOs of mononuclear **1** and **2** feature the $d_{z^2-y^2}$ and d_{z^2} and the $\pi[p_z(Au-P)$ and $\pi[p_z(Rh-P-C)$ characteristics, respectively. As a result of the metal−metal interaction, σ^*(d) and $\sigma(p_z)$ contribute to the HOMOs and LUMOs of homobinuclear **3** and **4** complexes, respectively. However, the Au and Rh participations are inevitably unequal in heterobinuclear **5** due to differences in the electronic properties of the two metal atoms. Comparing **5** to **7**, we found that the change of the bridgeheads from CH_2 to NH moieties slightly affects their electronic structures. The oxidation of **5**−**7** is mainly limited to the metal centers. It should be emphasized that **6** and **9**, having great Cl participation in the frontier occupied orbitals, differ from **7** and **10** and from **5** and **8** in many respects.

The simulated absorption spectra under the TD-DFT calculations agree well with experimental ones. We focused on the lower-energy $d_{z^2} \rightarrow p_z$ absorption bands. The bands for mononuclear **1** and **2** were calculated at 202 and 395 nm, respectively, and cause a large red shift in binuclear **3**−**7** due to the metal−metal interaction.

Geometry optimizations and bond-order and frequency calculations reveal the existence of weak metal−metal bonding in **3**−**7** in the ground states. This is also proved by such metal-centered transition absorptions. The two-electron oxidation of **5**−**7** results in the occurrence of Au−Rh σ single bonds in **8**−**10**. Upon excitation, the metal−metal distances in the excited states of **3**−**6** shorten, whereas the distance in **9** greatly lengthens. This closely correlates with the promotion of electrons into the bonding or antibonding orbitals of the metal centers.

The UMP2 calculations predicted that **1** and **2** have metal-localized $p_z \rightarrow d_{z^2-y^2}/d_{z^2}$ triplet emissive excited states. The charge transfer between the metal centers and ligands also contributes to the excited states. As a result of the metal−metal interaction, the charge transfers for homobinuclear **3** and **4** and heterobinuclear **5** are attributed to MC and MC/MMCT transitions, respectively.

Acknowledgment. This work is supported by the Key Program Projects of the National Nature Science Foundation of China (20431030), the Natural Science Foundation of China (20703015, 20573042, and 20671032), the Natural Science Foundation of Heilongjiang Province of China (B200601), the Youth Science Foundation of Heilongjiang Province of China (QC08C15), the Supporting Plan for Excellent Youth of Common Universities of Heilongjiang Province of China (1153G028), and the Science Foundation for Excellent Youth of Heilongjiang University of China (JC2006L2).

Supporting Information Available: Tables of experimental results for **5** using various methods, basis sets, and solvent-effect models. Tables of orbital contributions and geometry parameters for **1**−**10** in the ground states. Tables of absorptions and orbital information for **1**, **2**, **6**, and **9** under TD-DFT calculations. Figure of energy-level diagrams of molecular orbitals of **5**, **7**, **8**, and **10**. Figures of simulated absorption spectra for **1**−**5**. Figures of electron density diagrams for some featured absorptions and HOMOs/LUMOs in the excited states. This material is available free of charge via the Internet at http://pubs.acs.org.

IC801687W